Experimental investigation of TRS-483 reference dosimetry correction factors for Leksell Gamma Knife® Icon™ beams

Wille Häger[a)]
Department of Physics, Stockholm University, Stockholm SE-106 91, Sweden

Vaiva Kaveckyte
Radiation Physics, Department of Medical and Health Sciences, Linköping University, Linköping SE-581 85, Sweden
Department of Medical Radiation Physics and Nuclear Medicine, Karolinska University Hospital, Stockholm SE-171 76, Sweden

Hamza Benmakhlouf
Department of Medical Radiation Physics and Nuclear Medicine, Karolinska University Hospital, Stockholm SE-171 76, Sweden

(Received 6 April 2020; revised 22 September 2020; accepted for publication 29 September 2020; published 21 November 2020)

Purpose: Radiosurgery using the Leksell Gamma Knife® (LGK) Icon™ is an established technique used for treating intracranial lesions. The largest beam field size the LGK Icon can produce is a 16 mm diameter sphere. Despite this, reference dosimetry on the LGK Icon is typically performed using ionization chambers calibrated in 10×10 cm^2 fields. Furthermore, plastic phantoms are widely used instead of liquid water phantoms. In an effort to resolve these issues, the International Atomic Energy Agency (IAEA) in collaboration with American Association of Physicists in medicine (AAPM) recently published Technical Report Series No. 483 (TRS-483) as a Code of Practice for small-field dosimetry. TRS-483 includes small-field correction factors, $k_{Q_{msr},Q_0}^{f_{msr},f_{ref}}$, intended to account for the differences between setups when using small-field modalities such as the LGK Icon, and conventional setups. Since the publication of TRS-483, at least three new sets of values of $k_{Q_{msr},Q_0}^{f_{msr},f_{ref}}$ for the LGK Icon have been published. The purpose of this study was to experimentally investigate the published values of $k_{Q_{msr},Q_0}^{f_{msr},f_{ref}}$ for commonly used phantom and ionization chamber (IC) models for the LGK Icon.

Methods: Dose-rates from two LGK units were determined using acrylonitrile butadiene styrene (ABS) and Certified Medical Grade Solid Water® (SW) phantoms, and PTW 31010 and PTW 31016 ICs. Correction factors were applied, and the resulting dose-rates compared. Relative validity of the correction factors was investigated by taking the ratios of dose-rate correction factor products. Additionally, dose-rates from the individual sectors were determined in order to calculate the beam attenuation caused by the ABS phantom adapter.

Results and Conclusions: It was seen that the dose-rate is underestimated by at least 1% when using the ABS phantom, which was attributed to fluence perturbation caused by the IC and phantom adapter. Published correction factors $k_{Q_{msr},Q_0}^{f_{msr},f_{ref}}$ account for these effects to varying degree and should be used. The SW phantom is unlikely to underestimate the dose-rate by more than 1%, and applying $k_{Q_{msr},Q_0}^{f_{msr},f_{ref}}$ could not be shown to be necessary. Out of the two phantom models, the ABS phantom is not recommended for use in LGK reference dosimetry. The use of newly published values of $k_{Q_{msr},Q_0}^{f_{msr},f_{ref}}$ should be considered. © *2020 The Authors. Medical Physics* published by Wiley Periodicals LLC on behalf of American Association of Physicists in Medicine [https://doi.org/10.1002/mp.14561]

Key words: code of practice, Leksell Gamma Knife, reference dosimetry, phantom, $k_{Q_{msr},Q_0}^{f_{msr},f_{ref}}$

1. INTRODUCTION

Stereotactic radiosurgery using the Leksell Gamma Knife® (LGK, Elekta Instrument AB, Stockholm, Sweden) is a well-established modality used to treat a multitude of intracranial lesions. Currently there are more than 300 LGK centers worldwide treating more than 80 000 patients annually.[1] The LGK Icon™ produces a radiation beam via 192 ^{60}Co sources which are evenly distributed along a conical surface. The conical surface is divided into eight sectors which can be individually programmed to align with circular collimators yielding fields with diameters 4, 8, or 16 mm. The ^{60}Co beams coincide at a focal point, resulting in a small composite field with steep dose gradients.

While the LGK Icon boasts highly conformal dose distributions, the amount of absorbed dose in the patient is a subject of controversy. The LGK Icon cannot realize the reference field conditions in terms of field size, geometry, and phantom material advocated in clinically used Codes of Practice (CoPs), for example, Technical Reports Series No. 398 (TRS-398) published by the International Atomic Energy Agency (IAEA), and Task Group 51 (TG-51) published by the American Association of Physicists in Medicine (AAPM).[2,3] In particular, the reference field size of 10 cm ×

10 cm cannot be conceived by the LGK Icon, whose largest field is 16 mm in diameter. It is known that as the field size gets small (field half width or field radius <~2 cm for 6–15 MV photon beams; <~0.6 cm for ^{60}Co beams), small-field dosimetric phenomena emerge, leading to an underestimation of dose output if not accounted for.[4–7] The issues of small fields are not unique to the LGK Icon and are present in other radiosurgery modalities such as the CyberKnife® and TomoTherapy® Hi-ART® (Accuray, Inc., Sunnyvale, CA, USA), as well as linear accelerators with micro multi-leaf collimators.

In the absence of formal CoPs for small-field dosimetry, methodology for LGK reference dosimetry has historically been decided independently by clinics. Typically, LGK Icon dose-rates are determined using ionization chambers (ICs) calibrated in conventional reference conditions (i.e., according to TRS-398 or TG-51) along with spherical plastic phantoms in a 16 mm diameter field, or using an air kerma-based approach, that is, Task Group 21 (TG-21).[8] There is thus a mismatch in field size, geometry, and phantom material, for which the calibration coefficients of the ICs are obtained.

A formalism was published by Alfonso et al.[9] with the intent of resolving the issue of dosimetry on machines where replication of reference conditions is not possible. The formalism introduced a concept of machine-specific reference (msr) fields and a small-field correction factor $k_{Q_{msr},Q_0}^{f_{msr},f_{ref}}$ linking calibration conditions with machine conditions, where $k_{Q_{msr},Q_0}^{f_{msr},f_{ref}}$ is defined as the ratio of calibration coefficients for an IC under msr conditions and calibration conditions. As the name implies, the msr field acts as a reference field and is uniquely defined for each type of machine. For the LGK Icon, the msr field is defined as the composite field constructed when all sectors are aligned with 16 mm collimators, which is the largest conceivable field. With msr fields defined, it is the vision that small-field effects can be accounted for by applying the $k_{Q_{msr},Q_0}^{f_{msr},f_{ref}}$ correction factor. The formalism has been adopted into the Technical Report Series No. 483 (TRS-483, IAEA) CoP intended for dosimetry of small static fields.[10,11] At the time of publication of TRS-483, only one set of $k_{Q_{msr},Q_0}^{f_{msr},f_{ref}}$ values had been published, and are therefore the only values included in the CoP.[12] Since the publication of TRS-483, at least three additional sets of $k_{Q_{msr},Q_0}^{f_{msr},f_{ref}}$ values have been published, all of which exhibit slight differences in methodology and results.[13–15] Despite a surge of interest in small-field correction factors for the LGK Icon, few attempts have been made to verify them experimentally.[16,17] During commissioning of an LGK Icon at Karolinska University Hospital, Stockholm, Sweden, in September 2018, dose-rates were determined using an acrylonitrile butadiene styrene (ABS) phantom, and a Certified Medical Grade Solid Water® (SW) phantom. A discrepancy in determined dose-rates between using the two phantom models was seen (M. Fager, personal communication, 25 April 2019). While the discrepancy was expected, its magnitude did not match the corrections predicted by the factors from TRS-483. In other words, the correction factors in TRS-483 appeared to be inaccurate for this case.

The aim of this study was to experimentally investigate all published correction factors for two phantom types and two IC models commonly used in LGK Icon radiation dosimetry, and to assess whether the newly published correction factors should be considered for inclusion in TRS-483.

2. MATERIALS AND METHODS

According the TRS-483 CoP, absorbed dose to water in absence of a detector, $D_{w,Q_{msr}}^{f_{msr}}$, is determined by.

$$D_{w,Q_{msr}}^{f_{msr}} = M_{Q_{msr}}^{f_{msr}} N_{D,w,Q_0}^{f_{ref}} k_{Q_{msr},Q_0}^{f_{msr},f_{ref}} \quad (1)$$

where

f_{msr} is the machine-specific reference field (= all eight sectors aligned with 16 mm collimators for the LGK Icon);

f_{ref} is the reference field used when calibrating the detector at the standards laboratory at a depth of 10 g cm^{-2} in water in a source-to-axis setup;

Q_{msr} and Q_0 are the beam qualities in the msr and calibration fields. While ^{60}Co is typically used in both cases, small-field effects may cause the beam quality at the point of measurement in the msr field to differ from the calibration beam quality;

$D_{w,Q_{msr}}^{f_{msr}}$ is the absorbed dose (Gy) to water in the absence of a detector, in the field f_{msr} in a beam with quality Q_{msr};

$M_{Q_{msr}}^{f_{msr}}$ is the measured charge (C) in the field f_{msr} with beam quality Q_{msr}, corrected for temperature, pressure, humidity, polarity effects, recombination effects, and electrometer;

$N_{D,w,Q_0}^{f_{ref}}$ is the detector calibration coefficient (Gy C^{-1}) determined in the conventional reference field f_{ref} in a beam with quality Q_0;

$k_{Q_{msr},Q_0}^{f_{msr},f_{ref}}$ is a small-field correction factor that accounts for the differences in beam quality, field size, phantom material, detector, and overall geometry between the reference and the machine-specific conditions.

The small-field correction factor $k_{Q_{msr},Q_0}^{f_{msr},f_{ref}}$ is defined as the ratio of detector calibration coefficients in the msr and reference fields. By making the approximation that measured charge by a detector is proportional to average absorbed dose within the detector sensitive volume, $k_{Q_{msr},Q_0}^{f_{msr},f_{ref}}$ can be determined via.

$$k_{Q_{msr},Q_0}^{f_{msr},f_{ref}} = \frac{N_{D,w,Q_{msr}}^{f_{msr}}}{N_{D,w,Q_0}^{f_{ref}}} = \frac{D_{w,Q_{msr}}^{f_{msr}}/M_{Q_{msr}}^{f_{msr}}}{D_{w,Q_0}^{f_{ref}}/M_{Q_0}^{f_{ref}}} \approx \frac{D_{w,Q_{msr}}^{f_{msr}}/\bar{D}_{det,Q_{msr}}^{f_{msr}}}{D_{w,Q_0}^{f_{ref}}/\bar{D}_{det,Q_0}^{f_{ref}}}. \quad (2)$$

where all the individual factors of the right-most term of Eq. (2) can be numerically determined via Monte Carlo methods. The to date published values of $k_{Q_{msr},Q_0}^{f_{msr},f_{ref}}$ for two phantom and IC models are summarized in Table I.

Two PTW 31010 and two PTW 31016 ICs (PTW Freiburg GmbH, Freiburg, Germany) calibrated at either the Swedish Radiation Safety Authority, Stockholm, Sweden, or PTW Freiburg, Freiburg, Germany, were used in this study. These

TABLE I. Published values of $k_{Q_{msr},Q_0}^{f_{msr},f_{ref}}$ for two phantom and ionization chamber models.

Monte Carlo code	Johansson et al.[12] PENELOPE	Zoros et al.[13] EGSnrc	Mirzakhanian et al.[14] EGSnrc	Schaarschmidt et al.[15] GEANT4
	ABS phantom			
Includes adapter?	Yes	Yes	No	No
PTW T31010	1.015 (0.4%)	1.022 (0.8%)	1.024 (0.9%)	1.002* (1.8%)
PTW T31016	1.011 (0.4%)	1.023 (0.8%)	1.014 (0.9%)	1.006* (2.2%)
	SW phantom			
PTW T31010	1.004 (0.4%)	1.008 (0.8%)	1.009 (0.9%)	0.997 (1.8%)
PTW T31016	1.004 (0.4%)	1.005 (0.8%)	1.011 (0.9%)	1.005 (2.2%)

Combined Type A and Type B uncertainties are denoted in the parentheses (k = 2). All values were numerically determined. Inclusion of the ABS adapter in the simulated geometry is denoted. *A parallel detector orientation was used.

two IC models are commonly used in LGK Icon dosimetry, particularly in Europe and Asia. The specifications of the IC models are presented in Table II.

There are two phantom models commonly used for LGK Icon dosimetry: an acrylonitrile butadiene styrene (ABS) phantom and a Certified Medical Grade Solid Water® (SW) phantom (Fig. 1). Both phantom models are provided to LGK centers by the vendor (Elekta). The SW phantom is intended to be more equivalent to water than the ABS phantom in terms of mass density, electron density, and atomic composition. Still, the ABS phantom is more commonly used in clinics for economic reasons. Both phantom models are spherical with 16 cm diameters. The phantoms have slots for inserts with holes drilled according to the geometrical specifications of specific detector models. The phantoms attach to aluminum adapters specific to the phantom model. The adapters attach to the LGK Icon couch, projecting the phantoms onto the LGK Icon stereotactic space. Two ABS phantoms and one SW phantom were used in this study. One unique insert per IC-phantom combination was used, except for the 31010 IC - ABS phantom combination, where two duplicate inserts were available.

TABLE II. Specifications of the two ionization chamber models used in this study.

Directional dependency	≤ ±0.5% rotationally	≤ ±0.5% rotationally
Electrode material	Al 99.98	Al 99.98
IC model	PTW Type 31010	PTW Type 31016
Sensitive volume	0.125 cm^3	0.016 cm^3
Wall material	0.55 mm PMMA 0.15 mm graphite	0.57 mm PMMA 0.09 mm graphite
Electrode diameter	1.1 mm	0.3 mm

The small sensitive volumes and low-directional dependency make these ionization chambers appropriate for small-field dosimetry.

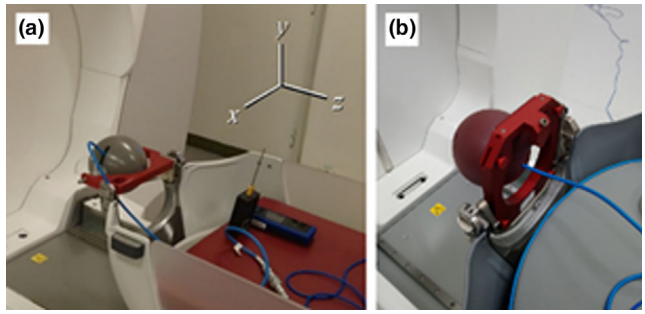

FIG. 1. The two phantom types and respective measurement setups used; (a) ABS phantom; (b) SW phantom. [Color figure can be viewed at wileyonlinelibrary.com]

The ABS phantom adapter is partially occluding the primary beam in sectors 3 and 7 [Fig. 2(a)], and has been shown to attenuate the beam by approximately 1%.[13,18] The studies by Johansson et al.[12] and Zoros et al.[13] included the ABS adapter in their simulations while the studies by Mirzakhanian et al.[14] and Schaarschmidt et al.[15] did not. The SW phantom adapter is not directly in the primary beam path and its effect on dose-rate is assumed to be negligible.

2.A. Detector orientation within the ABS phantom

There are two detector orientations commonly used in the ABS phantom (Fig. 3):

1. *Perpendicular* orientation: The detector is oriented perpendicular to the LGK Icon stereotactic *z*-axis, offset by 45° from the *xz*-plane. The correction factors by Johansson et al.[12] and Zoros et al.[13] were determined using the perpendicular orientation. Mirzakhanian et al.[14] determined correction factors using both detector orientations, though only the values determined using the perpendicular orientation are included in this study. If not explicitly noted, all ABS phantom measurements were performed using the perpendicular orientation in this study.

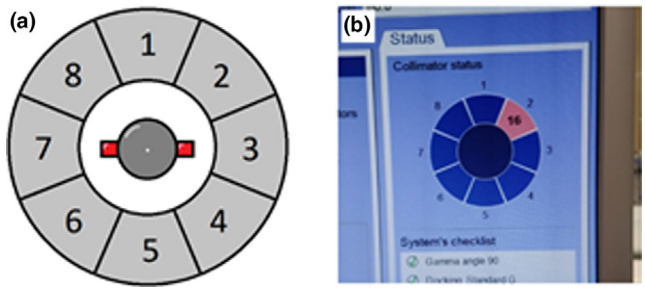

FIG. 2. (a) Cut-away view (not to scale) of the ABS phantom (gray disk) and phantom adapter (red squares) in the irradiation position. The beam focus is the white dot in the geometric center. b) Example of a custom dose plan (dose delivery view) designed for measuring the output of sector 2. [Color figure can be viewed at wileyonlinelibrary.com]

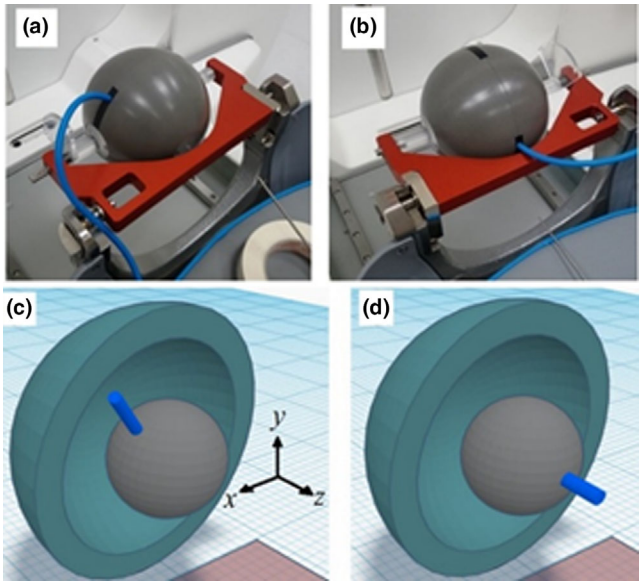

FIG. 3. The two detector orientations used with the ABS phantom: (a) perpendicular mode; (b) parallel mode (image has been horizontally flipped for clarity); (c)-(d) 3D-renders of the perpendicular and parallel mode, respectively. [Color figure can be viewed at wileyonlinelibrary.com]

2. *Parallel* orientation: The detector is oriented centrally and parallel to the *z*-axis. Note that the ABS adapter obstructs the detector from lying exactly in the *xz*-plane. The correction factors by Schaarschmidt et al.[15] were determined using the parallel orientation.

In both detector orientations, the sensitive volume of the IC is centered in the LGK Icon beam focus, however in the perpendicular orientation part of the primary beam impinges on the IC from behind.

Two LGK units were used in this study: one LGK Icon and one LGK Perfexion™. Both LGK units were located at Karolinska University Hospital, Stockholm, Sweden. The LGK Icon has on-board imaging capabilities in terms of a cone-beam computed tomography system, whereas the LGK Perfexion does not. Aside from dose-rate (i.e., source activity), the LGK Perfexion is dosimetrically identical to the LGK Icon in terms of beam quality and geometry. All determined dose-rates were corrected for the difference in source activity between the LGK Icon and LGK Perfexion, as well as the radioactive decay of the sources during the time span of this study.

Dose-rates were determined using Eq. (1) divided with time. Charge was integrated over 1 min using a PTW Unidos E Electrometer. Measurements were repeated until six consistent values were achieved while avoiding trends. Measured charge was corrected for temperature and pressure. Polarity and recombination effects were determined once for each IC. The electrometer, thermometer, and barometer were calibrated at SP Technical Research Institute of Sweden (SP). All ICs were pre-irradiated with at least 10 Gy, and were connected to the electrometer for at least 15 min before measurements. Leakage current was less than 0.1% of the total current. Chamber voltages of −400 V and +400 V were used for the 31010 and 31016 ICs, respectively.

The dose-rate determined with the 31010 IC and SW phantom was chosen as a baseline since this combination of equipment was the one routinely used in the clinic, even though it does not necessarily reflect the true dose-rate.

2.B. Ratios of dose-rates

The relative validity of the small-field correction factors was investigated by evaluating the ratio of phantom measurements, $\zeta^{x}_{a/b}$, and the ratio of detector measurements, $\xi^{a}_{x/y}$,

$$\zeta^{x}_{a/b} = \left[\frac{\dot{D}'_{\text{phan}.a}}{\dot{D}'_{\text{phan}.b}} \cdot \frac{k_{\text{phan}.a}}{k_{\text{phan}.b}}\right]_{\text{detector } x} \tag{3}$$

$$\xi^{a}_{x/y} = \left[\frac{\dot{D}'_{\text{det}.x}}{\dot{D}'_{\text{det}.y}} \cdot \frac{k_{\text{det}.x}}{k_{\text{det}.y}}\right]_{\text{phantom } a} \tag{4}$$

where $\dot{D}'$ is the determined dose-rate not multiplied with the small-field correction factor, and $k \equiv k^{f_{\text{msr}},f_{\text{ref}}}_{Q_{\text{msr}},Q_0}$ is the small-field correction factor, for phantom *a*,*b*, and detector *x*, *y*. The values of $\zeta^{x}_{a/b}$ and $\xi^{a}_{x/y}$ are expected to be unity if the values of k are accurate relative to each other.

2.C. Sector measurements

In order to investigate the attenuation caused by the ABS phantom adapter, the dose-rate of each sector of the LGK Icon was determined independently using both IC and phantom models and custom dose plans [Fig. 2(b)] where only one sector was open at a time. Both the perpendicular and parallel detector orientations were used with the ABS phantoms. The beam attenuation was calculated (see Bhatnagar et al.[18] for details) and an attenuation correction factor β was applied [Eq. (5)] to the values of $k^{f_{\text{msr}},f_{\text{ref}}}_{Q_{\text{msr}},Q_0}$ determined by Mirzakhanian et al.[14] to compensate for the absence of the ABS adapter in their simulations, resulting in a fifth set of correction factors.

$$\left[\mathbf{k}^{f_{\text{msr}},f_{\text{ref}}}_{Q_{\text{msr}},Q_0}\right]_{\beta\cdot\text{Mirzakhanian}} \equiv \beta \cdot \left[\mathbf{k}^{f_{\text{msr}},f_{\text{ref}}}_{Q_{\text{msr}},Q_0}\right]_{\text{Mirzakhanian}} \tag{5}$$

where $\left[\mathbf{k}^{f_{\text{msr}},f_{\text{ref}}}_{Q_{\text{msr}},Q_0}\right]_{\text{Mirzakhanian}}$ is the original set of values by Mirzakhanian et al.[14] The factor β was not applied to the set of correction factors by Schaarschmidt et al.[15] since their correction factors were determined using the parallel detector orientation. The beam output from each sector was also measured using the SW phantom to determine the relative source strength in each sector.

2.D. Uncertainty analysis

Uncertainty was calculated in concordance with the Guide of the Expression of Uncertainty in Measurement.[19] The uncertainty of the calibration coefficients $N_{D,w}$ was given in the calibration certificates by the Secondary Standards

Dosimetry Laboratory at the The Swedish Radiation Safety Authority. All uncertainties in this paper are expressed with coverage factor $k = 2$. No correlation between any uncertainties was assumed. Statistical significance was investigated using a two-sample *t*-test and the level of statistical significance was set to $p \leq 0.05$. Uncertainties considered in this study are presented in Table III under Results.

3. RESULTS

No significant differences in determined dose-rates were seen between using the two ABS phantoms, the two 31010-ABS phantom inserts, the two 31010 ICs, the two 31016 ICs, and the LGK Icon and LGK Perfexion units. The setups for measurements using these doublets of equipment were therefore treated identically, and the data were combined in the subsequent analysis. Uncertainties considered in this study are presented in Table III.

3.A. Small-field correction factors

Dose-rates normalized to the dose-rate determined with the 31010 IC and SW phantom are summarized in Fig. 4 and Table IV.

No significant difference was seen between the uncorrected dose-rates when using the 31010 and 31016 ICs with the SW phantom [Figs. 4(a) and 4(b)]. All correction factors (except Schaarschmidt et al.[15] for the 31010 IC) increased the dose-rate, but were not significantly different from the uncorrected value.

The uncorrected dose-rates when using the ABS phantoms [Figs. 4(c) and 4(d)] was significantly lower than when using the SW phantom for the 31010 IC (−2.2%). This also appeared to be the case for the 31016 IC (−1.3%), but was not significant. All correction factors appeared to yield dose-rates closer to the baseline for both ICs. For the 31010 IC, the correction factors by Zoros et al.[13] and Mirzakhanian et al.[14] yielded values close to the baseline (1.00 ± 0.014 and 1.00 ± 0.015, respectively). The value by Johansson et al.[12] also appeared to improve the uncorrected value (0.99 ± 0.012). For the 31016 IC, the correction factors Johansson et al.[12] and Mirzakhanian et al.[14] yielded values close to the baseline (1.00 ± 0.013 and 1.00 ± 0.015, respectively). For both ICs, the adapter-modified correction factors, β·Mirzakhanian et al.,[14] yielded values ~1% above the baseline, as did the correction factors by Zoros et al.[13] for the 31016 IC.

TABLE III. Uncertainties considered in this study.

Source of uncertainty	Uncertainty (%)	
Statistical (2σ)	31010-ABS	0.6
	31010-SW	0.3
	31016-ABS	0.8
	31016-SW	1.1
Electrometer		0.5
$N_{D,w}$		1.0
β		0.7
Total (excluding $k_{Q_{msr},Q_0}^{f_{msr},f_{ref}}$)	31010-ABS	1.3
	31010-SW	1.2
	31016-ABS	1.4
	31016-SW	1.6

Combined Type A and Type B uncertainties with a coverage factor k = 2 are displayed. The uncertainties of the $k_{Q_{msr},Q_0}^{f_{msr},f_{ref}}$ factors are presented in Table I.

3.B. Ratios of dose-rates

Values of $\zeta_{ABS/SW}$ and $\xi_{31010/31016}$ are summarized in Fig. 5 and Table V.

The ABS/SW-phantom ratio, $\zeta_{ABS/SW}$, only the uncorrected dose-rate for the 31010 IC was significantly below unity (−2.2%). For the 31010 IC [Fig. 5(a)], applying small-field correction factors improved all ratios, bringing them closer to unity, though tended to fall short by approximately 1%. The correction factors by Mirzakhanian et al.[14] modified with the adapter attenuation constant (+0.8%) performed the best, rendering a ratio of 1.00 ± 0.022. For the 31016 IC [Fig. 5(b)], applying small-field correction factors appeared to improve all ratios, with the correction factors by Zoros et al.[13] and the adapter-modified correction factors by Mirzakhanian et al.[14] performing the best, rendering ratios of 1.00 ± 0.021 and 1.00 ± 0.023, respectively.

The 31010/31016-IC ratio, $\xi_{31010/31016}$, of uncorrected dose-rates was within unity for all cases. None of the correction factors changed the ratio significantly.

3.C. Sector measurements

A reduction in measured beam output was seen in sectors 3 and 7 when measuring with the ABS phantom using a parallel detector orientation [Fig. 6(a)]. The value of β was determined to be 1.008 ± 0.007, corresponding to an average total percentage reduction in beam output by 0.8%. The average determined dose-rate was 1.5% less for the perpendicular orientation compared to the parallel orientation, which seemed to emanate from a reduction in beam output from sectors 7 and 8 [Fig. 6(b)]. No apparent reduction in output was seen in any sector when measuring with the SW phantom [Fig. 6(c)].

4. DISCUSSION

4.A. Baseline vs. the true dose-rate

The dose-rate determined with the SW phantom and 31010 IC was used as a baseline for mathematical comparisons. This combination of equipment is commonly used in clinics, and it was suspected that the SW phantom yields dose-rates closer to the true value than the ABS phantom does. Nevertheless, the baseline should not be interpreted as the true dose-rate. Ideally a reference acting as the true dose-rate would have been used. Microfluidic calorimeters for the

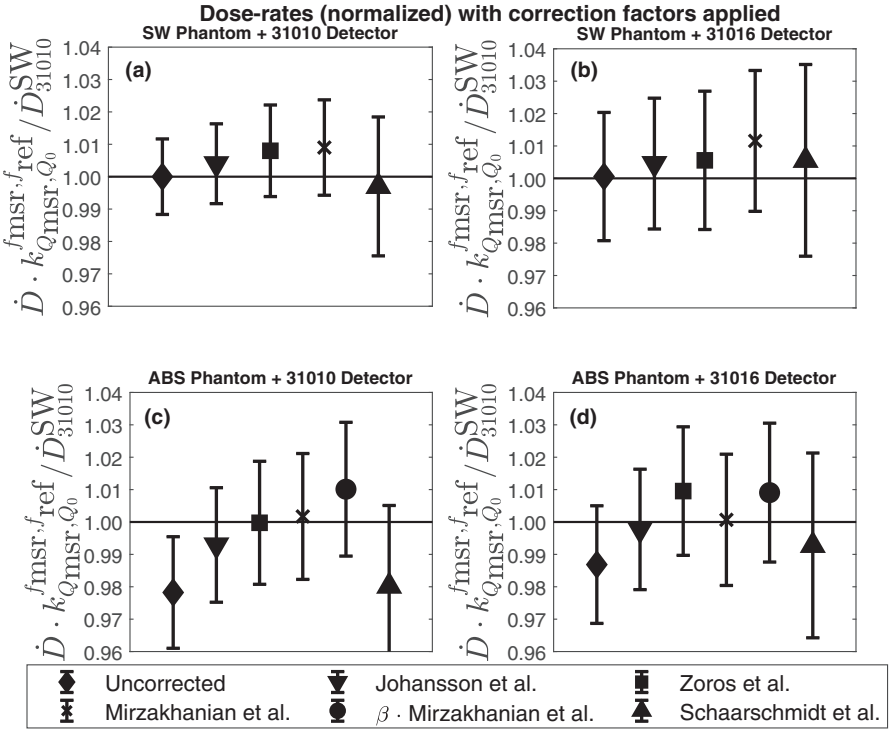

FIG. 4. Determined dose-rates normalized to the baseline for the SW and ABS phantoms, along with the 31010 and 31016 ICs. The uncertainty bars correspond to the combined Type A and Type B uncertainty with k = 2.

TABLE IV. Determined dose-rates (normalized), with applied small-field correction factors, for the ABS and SW phantoms, and 31010 and 31016 ionization chambers.

	$\dot{D} \cdot k_{Q_{msr},Q_0}^{f_{msr},f_{ref}} / \dot{D}_{31010}^{SW}$	
	PTW 31010	PTW 31016
SW phantom		
Uncorrected	1 ± 0.012	1.00 ± 0.020
Johansson et al.[12]	1.00 ± 0.012	1.01 ± 0.020
Zoros et al.[13]	1.01 ± 0.014	1.01 ± 0.021
Mirzakhanian et al.[14]	1.01 ± 0.015	1.01 ± 0.022
Schaarschmidt et al.[15]	1.00 ± 0.021	1.01 ± 0.030
ABS phantom		
Uncorrected	0.98 ± 0.017	0.99 ± 0.018
Johansson et al.[12]	0.99 ± 0.018	1.00 ± 0.019
Zoros et al.[13]	1.00 ± 0.019	1.01 ± 0.020
Mirzakhanian et al.[14]	1.00 ± 0.019	1.00 ± 0.020
β·Mirzakhanian et al.[14]	1.01 ± 0.021	1.01 ± 0.021
Schaarschmidt et al.[15]	0.98 ± 0.025	0.99 ± 0.029

purpose of small-field dosimetry have been investigated, but their practical feasibility remains to be proven.[20] Thermoluminescent dosimeters were opted out of usage in this study due to their intrinsically high uncertainties, and the use of other detectors was limited by the available phantom inserts. It was assumed that the SW phantom yields dose-rates closer to the true value than the ABS phantom due to the absence of fluence perturbation caused by the IC and phantom adapter. Judging by the published values of $k_{Q_{msr},Q_0}^{f_{msr},f_{ref}}$, the true dose-rate is still underestimated by the SW phantom by roughly 1%, though this could not be proven in this study.

4.B. The SW phantom vs. the ABS phantom

No significant difference in detector response was seen between the 31010 and 31016 IC models when using the SW phantom. The parallel detector orientation was used with the SW phantom, and perhaps the difference in electrode diameter between the two ICs plays a lesser role in this case. The LGK radiation field is azimuthally symmetric, and there may less beam perturbation caused by the electrode itself when in the parallel orientation. The similar performance of the two IC models with the SW phantom was predicted by most published data, reporting values of $\left(k_{31010/31016}\right)\text{SW} \approx 1$.[12–14]

For the ABS phantoms, the determined dose-rates were seen to be on average lower than the dose-rates determined with the SW phantom. This can mainly be attributed to three reasons:

- *Differences in material properties (electron density, mass density).* The role of phantom material electron density on $k_{Q_{msr},Q_0}^{f_{msr},f_{ref}}$ has been shown to follow a linear relationship.[14] Different values for electron densities were used in the studies by Johansson et al.[12] and Zoros et al.[13], and this fact may therefore be reflected in the different values of $k_{Q_{msr},Q_0}^{f_{msr},f_{ref}}$. Using the method reported in Mirzakhanian et al.[14], the difference in $k_{Q_{msr},Q_0}^{f_{msr},f_{ref}}$ is less than 0.4%. Though it should be pointed out that the true

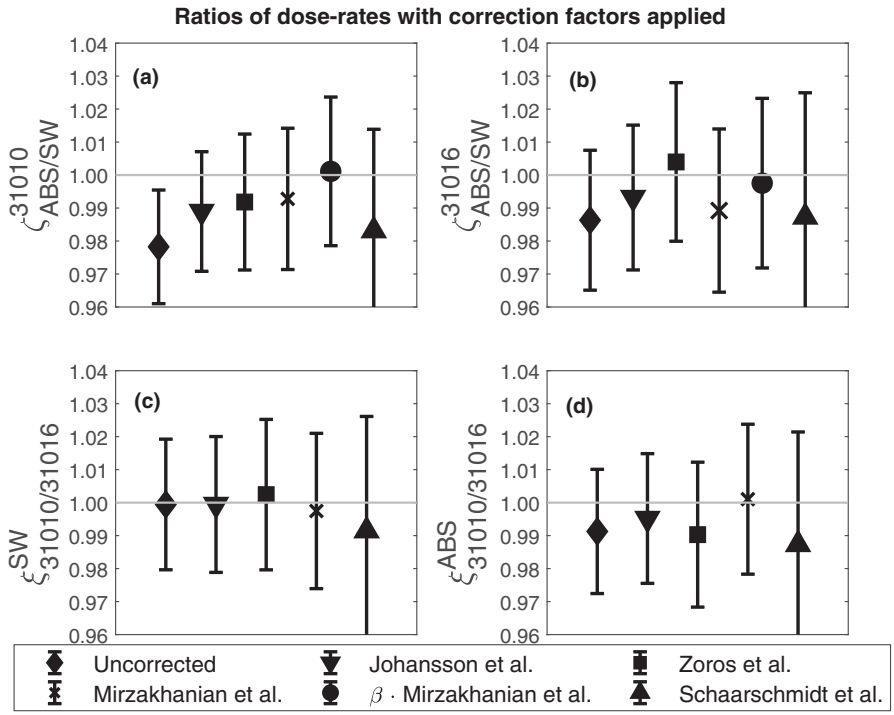

FIG. 5. Ratios of determined dose-rates with applied small-field correction factors using SW and ABS phantom models, and 31010 and 31016 ionization chamber models. The uncertainty bars correspond to the combined Type A and Type B uncertainty with k = 2.

TABLE V. Ratios of determined dose-rates with applied small-field correction factors using SW and ABS phantom models, and 31010 and 31016 ionization chamber models.

	$\zeta^{31010}_{ABS/SW}$	$\zeta^{31016}_{ABS/SW}$	$\xi^{SW}_{31010/31016}$	$\xi^{ABS}_{31010/31016}$
Uncorrected	0.98 ± 0.017	0.99 ± 0.021	1.00 ± 0.020	0.99 ± 0.019
Johansson et al.[12]	0.99 ± 0.018	0.99 ± 0.022	1.00 ± 0.021	1.00 ± 0.020
Zoros et al.[13]	0.99 ± 0.021	1.00 ± 0.024	1.00 ± 0.023	0.99 ± 0.022
Mirzakhanian et al.[14]	0.99 ± 0.021	0.99 ± 0.025	1.00 ± 0.024	1.00 ± 0.023
β·Mirzakhanian et al.[14]	1.00 ± 0.023	1.00 ± 0.026	*	†
Schaarschmidt et al.[15]	0.98 ± 0.031	0.99 ± 0.038	0.99 ± 0.035	0.99 ± 0.034

*The adapter attenuation factor β is not applicable when using the SW phantom.
†The adapter attenuation factor β is canceled out in this case.

values of the electron density of the ABS and SW materials are not conclusively known, and the impact on $k^{f_{msr},f_{ref}}_{Q_{msr},Q_0}$ could thus be greater than 0.4%. The effect of mass density on $k^{f_{msr},f_{ref}}_{Q_{msr},Q_0}$ has not been investigated in particular, but it is not likely to contribute the difference significantly given the close values of the reported mass densities between the SW and ABS phantom models. Novotny et al.[21] investigated the constancy of mass density of 13 ABS phantoms and saw a percentage output variation in the range from −0.72% to 0.48%. However, in this study, the two ABS phantoms performed remarkably similarly ($\bar{D}_{ABS1}/\bar{D}_{ABS2} = 1.000 \pm 0.016$).

- *Attenuation caused by the ABS adapter.* The attenuation caused by the ABS adapter was determined to be 0.8%. This is comparable with previous studies which determined the attenuation to be on the order of 1%.[13,18] Meanwhile, the SW phantom adapter does not attenuate the beam directly. This emphasizes the importance of including the ABS adapter when determining $k^{f_{msr},f_{ref}}_{Q_{msr},Q_0}$, and perhaps to a greater extent, the unfitness of the ABS phantom for use in reference dosimetry.
- *Difference in detector orientation.* The measurements using the SW and ABS phantom were performed with the parallel and perpendicular detector orientation respectively. When the detector is in the perpendicular orientation, the IC stem and cable are directly in the primary beam path. Stem effects caused by the IC stem being in the primary beam have been shown to artificially increase the detector signal.[22] Though in this study an overall decrease was seen, suggesting that beam fluence perturbation caused by the IC plays a greater role in this case.

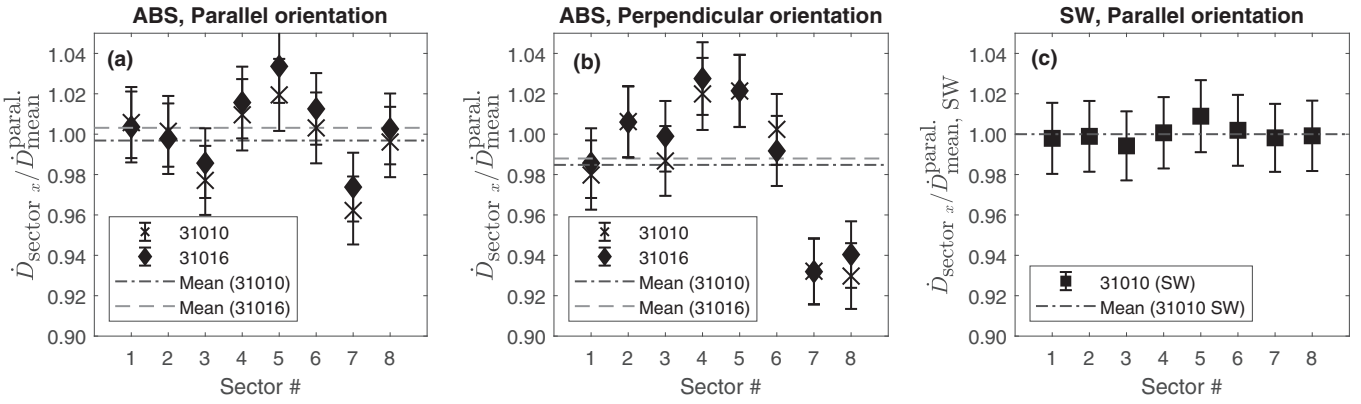

FIG. 6. Determined dose-rates for the individual sectors normalized to the mean of the parallel measurements; a) When using the parallel orientation; b) When using the perpendicular orientation; c) As well as a control using the SW phantom. The uncertainty bars correspond to the combined Type A and Type B uncertainty with k = 2.

If the material differences between the phantoms are neglected by setting the material factor $k_{\text{material}} = 1$, and we only consider the impact of the phantom adapter, k_{adapter}, and the detector orientation, $k_{\text{orientation}}$, factoring the three contributions $(k_{\text{total}} = k_{\text{material}} \cdot k_{\text{adapter}} \cdot k_{\text{orientation}} = 1 \cdot 1.008 \cdot 1.015)$ for the ABS phantom yields a -2.3% expected difference in determined dose-rates between using the ABS and SW phantom. This agrees with the difference between the phantom models seen in this study for the 31010 IC ($-2.2\% \pm 1.7\%$), but likely to a lesser extent with the 31016 IC ($-1.3\% \pm 1.8\%$). Since neither the phantom material properties nor the beam attenuation caused by the ABS adapter should depend on the IC model used, it appears the orientation factor (=1.5%) for the 31016 IC has been overestimated. The output differences for the two detector orientations were determined as a secondary objective from the sector tests in this study, which were only performed once per orientation and IC and may be considered statistically weak. Indeed, Mirzakhanian et al.[14] investigated the difference in beam perturbation caused by the IC stem, wall, electrode, cavity, and volume averaging via MC simulations, and instead saw a 0.8% decrease in detector response for the 31016 IC for the perpendicular orientation as compared to the parallel orientation. This value agrees with the dose-rate discrepancies seen in this study. It is clear the perpendicular detector orientation will decrease the apparent dose-rate, and this should be clarified in CoPs.

4.C. Comparison of $k_{Q_{msr},Q_0}^{f_{msr},f_{ref}}$ values

For the ABS phantom, when using the perpendicular orientation, the dose-rate is underestimated by at least 2% and 1% for the 31010 and 31016 ICs, respectively, if not corrected for. The $k_{Q_{msr},Q_0}^{f_{msr},f_{ref}}$ values included in TRS-483 improve the estimated dose-rates for both ICs, yielding values close to the SW-determined dose-rates (though it should be noted that only the values of $k_{Q_{msr},Q_0}^{f_{msr},f_{ref}}$ determined by Johansson et al.[12] are included in TRS-483, hence the CoP lacks any values of $k_{Q_{msr},Q_0}^{f_{msr},f_{ref}}$ intended for the parallel detector orientation). The ABS phantom along with the TRS-483 CoP may therefore serve as an economical compromise in lieu of using a SW phantom. However, if the true dose-rate is ~1% greater than the SW-determined dose-rate as predicted by most published values of $k_{Q_{msr},Q_0}^{f_{msr},f_{ref}}$, then the values of $k_{Q_{msr},Q_0}^{f_{msr},f_{ref}}$ by Zoros et al.[13] and Mirzakhanian et al.[14] may be more appropriate for the ABS phantom. Modifying the latter values to account for the ABS adapter may further yield dose-rates closer to the true value, as supported by the values of phantom ratios $\phi_{\text{ABS/SW}}$, but this remains to be proven. Extending the study by Mirzakhanian et al.[14] to include the ABS adapter in their simulations would be of interest. Noteworthy is the similarity in determined dose-rates of the sectors not obstructed by the ABS adapter when using the ABS phantom in the parallel orientation and the SW phantom [Fig. 6(a)]. Indeed, the differences in material properties seemed to have a negligible impact on $k_{Q_{msr},Q_0}^{f_{msr},f_{ref}}$ since the attenuation by the ABS adapter combined with the difference in detector orientation manages to fully account for the difference in determined dose-rates between using the SW and ABS phantoms. This implies that the detector orientation and thus fluence perturbation plays a greater role than perhaps expected, and that the ABS phantom may be able to perform similar to the SW phantom if the ABS adapter was modified not to occlude the primary beam and to force a parallel detector orientation. Thorough investigation of the difference in detector response between the two orientations may shed light on this question.

The small-field correction factors for the SW phantom published in TRS-483 do not deviate from unity significantly, nor do the factors determined by Zoros et al.[13] or Schaarschmidt et al.[15] and justifying their use may be difficult in their current state. The factors by Mirzakhanian et al.[14] while significantly greater than unity could still not be proven to be useful in this study. These facts speak in favor of using the SW phantom.

The correction factors by Schaarschmidt et al.[15] were not useful given their large uncertainties. Their correction factors for the ABS phantom were determined using the parallel

detector orientation but were still included in this study for elucidating on the issues of detector orientation ambiguity.

Differences in published values of $k_{Q_{msr},Q_0}^{f_{msr},f_{ref}}$ may be traced to differences in; *code*: all groups used different Monte Carlo codes; *geometry*: for example, inclusion of the ABS adapter; *detector modeling*: the exact specifications of the ICs are not publicly known and various degrees of simplifications may have been used; *phantom material specifications*: see Table II; *reference field conditions*: when determining $D_{w,Q_0}^{f_{ref}}$ and $\bar{D}_{det,Q_0}^{f_{ref}}$ in Eq. (2), only Johansson et al.[12] and Zoros et al.[13] used the same reference field conditions as those defined in TRS-398 (and thus the same reference conditions the ICs used were calibrated under) while Mirzakhanian et al.[14] and Schaarschmidt et al.[15] both defined the source-surface distance as 100 cm instead of the source-detector distance. Furthermore, Schaarschmidt et al.[15] used a reference depth of 10 g cm^{-2} instead of 5 g cm^{-2}. The impact of many of these differences is debatable, but nevertheless serves as a testament for the need of standardizing LGK Icon dosimetry protocols.

4.D. In practice

Care must be taken when using the ABS phantom for LGK Icon dosimetry, based on the detector orientation ambiguity and the adapter beam attenuation. The ambiguity of detector orientation when using the ABS phantom has resulted in at least one LGK dosimetry study using the parallel orientation, but applying the small-field correction factors from TRS-483 (which are intended for the perpendicular orientation).[16] Likewise, the factor $k_{Q_{msr},Q_0}^{f_{msr},f_{ref}}$ itself has been determined for different detector orientations among published studies. The inconsistency of detector orientation use is traced to the fact that the design of the ABS phantom allows for both detector orientations, as well as the absence of any mention of detector orientation in the TRS-483 CoP. If the ABS phantom is used, it should be clearly defined which detector orientation to use. Care must also be taken to ensure the correction factors are applicable to the chosen detector orientation. Unfortunately, this is currently not possible if relying solely on the TRS-483 CoP.[10] Out of the two phantom models investigated in this study, the SW phantom is recommended for LGK Icon dosimetry since the deviation from the true dose-rate is not expected to exceed 1% when using 31010 or 31016 ICs. The determination of dose-rate also experienced less dependence on IC model when the SW phantom was used, which is most likely a consequence of the parallel detector orientation. The ambiguity of detector orientation is eliminated when using the SW phantom, as the design only allows for a parallel detector orientation. Lastly, the SW phantom adapter does not occlude the primary beam path at all.

4.F. Comparison to other work

Drzymala et al.[16] conducted a round-robin study comparing TG-21, TG-51, TG-51 modified with the correction factors by Johansson et al.[12] as well as in-air measurements. Four phantoms and two ICs were used, and included the ABS and SW phantom, along with one 31010 IC. The TG-21 protocol with the ABS phantom was used as a reference. Dose-rates within 1.5% of the reference were seen in 88% of the cases for TG-21, 70% of the cases for TG-51, and 93% of the cases for the modified TG-51, implying that the correction factors by Johansson et al.[12] are accurate, even though it appears the parallel instead perpendicular detector orientation was used for the ABS measurements. Noteworthy is that the average dose-rate determined using the SW phantom was ~1% *lower* than the TG-21/ABS reference.

Mirzakhanian et al.[17] recently investigated TRS-483 using the correction factors by Mirzakhanian et al.[14] and compared it to TG-21 and TG-51. Three phantoms and three ICs were used, and included the ABS and SW phantoms and a 31010 IC. On average, dose-rates determined using TG-51 were 1.6% and 1.2% lower than those determined with TG-21 and TRS-483. Applying the correction factors yielded dose-rates consistent within 0.4%. For the 31010 IC, the average dose-rate was ~1.7% higher when using the SW phantom as compared to the ABS phantom when using the TG-51 protocol. For the ABS phantom, the dose-rates were also on average 1.6% greater when using the parallel detector orientation as opposed to the perpendicular orientation. The results presented by Mirzakhanian et al.[17] agree with this study, in that applying the correction factors by Mirzakhanian et al.[14] accounted for the differences between the SW phantom and ABS phantom.

4.E. Clinical implication

Many LGK centers worldwide rely on the ABS phantom along with either 31010 or 31016 ICs or other small IC models such as the Exradin A16, for reference dosimetry. It can be assumed that small-field correction factors have not been widely applied, meaning that clinical dose-rates are at least 1–2% below the true dose-rate, leading to a corresponding overdosage of patients. Furthermore, while the msr field is sometimes used clinically, it is rarely ever used exclusively. Clinical fields are shaped using a combination of "shots," where each shot consists of solely, or a combination of, the 4, 8, and 16 mm diameter fields. Individual sectors may also be blocked completely. Small-field dosimetric effects become more prominent with decreased field size. For this reason, output factors (OF) for the 4 and 8 mm diameter fields, using the msr field as a reference, have been determined numerically and experimentally and are included in TRS-483.[13,23] The values of the OFs are in the order of several percent which the reference small-field error propagates throughout. Clearly, the true absorbed dose in patients is of much uncertainty, and accurate determination of the reference dose-rate is the first step in decreasing it.

4.F. Future work

While published values of $k_{Q_{msr},Q_0}^{f_{msr},f_{ref}}$ exist for a variety of phantom and IC models, only two phantom models and two

IC models were used in this study. The SW and ABS phantoms are de facto standard phantoms for use in LGK Icon dosimetry, though alternatives have been proposed and investigated.[16,24–26] Likewise, the 31010 and 31016 IC models are used in most LGK centers in Europe and Asia. Meanwhile, LGK centers in North America tend to use Exradin A16 ICs, which unfortunately was not available in this study, but would have been of great interest to investigate given the relatively large values of $k_{Q_{msr},Q_0}^{f_{msr},f_{ref}}$ determined for the A16 IC for both phantom models. Additionally, thorough experimental investigation of the difference between the parallel and perpendicular detector orientations for various IC models would be of great interest.

5. CONCLUSION

Dose-rates were determined using two phantom models and two ionization chamber models, and five different sets of small-field correction factors were applied. Small-field correction factors $k_{Q_{msr},Q_0}^{f_{msr},f_{ref}}$ appear useful for dosimetry with the ABS phantom but should be used carefully. For the SW phantom, they may be difficult to justify unless more precise dosimetry can be performed. The ABS phantom is not recommended for LGK Icon reference dosimetry due to the ambiguity of detector orientation and the beam attenuating phantom adapter, leading to a likely underestimation of dose-rate. The SW phantom is recommended for LGK Icon radiation reference dosimetry due to the forced parallel detector orientation and attenuation-free phantom adapter. Detector orientation and phantom adapter type seem to be more relevant than phantom material or ionization chamber model. The correction factors by Zoros et al.[13] and Mirzakhanian et al.[14] performed at least as well as the correction factors in TRS-483 and should be considered for use in LGK dosimetry.

ACKNOWLEDGMENTS

The authors are most grateful to Jonas Johansson for lending equipment and for valuable insights and discussions.

CONFLICT OF INTEREST

The authors have no relevant conflict of interest to disclose.

[a]Author to whom correspondence should be addressed. Electronic mail: wille.hager@fysik.su.se; Telephone: +46735236135.

REFERENCES

1. Leksell Gamma Knife Society. Gamma Knife Radiosurgery Hits Half-Century Mark with over a Million Patients Treated. https://www.elekta.com/meta/press-all.html?id=B7A42A48AE8242B9. Accessed February 19, 2019.
2. Andreo P, Burns DT, Hohlfeld K, et al.Absorbed Dose Determination in External Beam Radiotherapy. Technical Reports Series No. 398. Vienna: International Atomic Energy Agency; 2000.
3. Almond PR, Biggs PJ, Coursey BM, et al. AAPM's TG-51 protocol for clinical reference dosimetry of high-energy photon and electron beams. *Med Phys*. 1999;26:1847–1870.
4. Sanchez-Doblado F, Hartmann GH, Pena J, Rosello JV, Russiello G, Gonzalez-Castano DM. A new method for output factor determination in MLC shaped narrow beams. *Phys Med*. 2007;23:58–66.
5. Das IJ, Ding GX, Ahnesjo A. Small fields: nonequilibrium radiation dosimetry. *Med Phys*. 2008;35:206–215.
6. Aspradakis MM, Byrne JP, Palmans H, et al. IPEM report 103: small field MV photon dosimetry. *Int Atomic Energy Agency*. 2010; 41–42.
7. Li XA, Soubra M, Szanto J, Gerig LH. Lateral electron equilibrium and electron contamination in measurements of head-scatter factors using miniphantoms and brass caps. *Med Phys*. 1995;22:1167–1170.
8. Schulz RJ, Almond PR, Cunningham JC, et al. A protocol for the determination of absorbed dose from high-energy photon and electron beams (AAPM TG-21). *Med Phys*. 1983;10:741–771.
9. Alfonso R, Andreo P, Capote R, et al. A new formalism for reference dosimetry of small and nonstandard fields. *Med Phys*. 2008;35: 5179–5186.
10. Alfonso R, Andreo P, Capote R, et al. Dosimetry of Small Static Fields Used in External Beam Radiotherapy. Technical Reports Series No. 483. Vienna: International Atomic Energy Agency; 2017.
11. Palmans H, Andreo P, Huq MS, Seuntjens J, Christaki KE, Meghzifene A. Dosimetry of small static fields used in external photon beam radiotherapy: summary of TRS-483, the IAEA–AAPM international Code of Practice for reference and relative dose determination. *Med Phys*. 2018;45:e1123–e1145.
12. Johansson J, Gorka B, Novotny J, et al. *Plenary Oral Presentation at the 16th International Meeting of the Leksell Gamma Knife® Society*. Sydney: 2012:69.
13. Zoros E, Moutsatsos A, Pappas EP, et al. Monte Carlo and experimental determination of correction factors for Gamma Knife Perfexion small field dosimetry measurements. *Phys Med Biol*. 2017;62: 7532–7555.
14. Mirzakhanian L, Benmakhlouf H, Tessier F, Seuntjens J. Determination of factors for ion chambers used in the calibration of Leksell Gamma Knife Perfexion model using EGSnrc and PENELOPE Monte Carlo codes. *Med Phys*. 2018;45:1748–1757.
15. Schaarschmidt T, Kim TH, Kim YK, Yang HJ, Chung H. GEANT4-based Monte Carlo simulation of beam quality correction factors for the Leksell Gamma Knife Perfexion. *J Korean Phys Soc*. 2018;73: 1814–1820.
16. Drzymala RE, Alvarez PE, Bednarz G, et al. A round-robin gamma stereotactic radiosurgery dosimetry interinstitution comparison of calibration protocols. *Med Phys*. 2015;42:6745–6756.
17. Mirzakhanian L, Sarfehnia A, Seuntjens J. Experimental validation of recommended msr-correction factors for the calibration of Leksell Gamma Knife® IconTM unit following IAEA TRS-483. *Phys Med Biol*. 2020;65:065003.
18. Bhatnagar JP, Novotny J Jr, Quader MA, Bednarz G, Huq MS. Unintended attenuation in the Leksell Gamma Knife Perfexion calibration-phantom adaptor and its effect on dose calibration. *Med Phys*. 2009; 36:1208–1211.
19. Metrology BJC for G in. Evaluation of Measurement Data – Guide to the Expression of Uncertainty in Measurement. Sévres: WG1; 2008. https://www.bipm.org/utils/common/documents/jcgm/JCGM_100_2008_E.pdf.
20. Schaarschmidt T, Kim YK, Chung H-T. Feasibility study of a small field detector based on a microfluidic calorimeter. *J Korean Phys Soc*. 2019;74:630–636.
21. Novotny J Jr, Bhatnagar JP, Chung HT, et al. Assessment of variation in Elekta plastic spherical-calibration phantom and its impact on the Leksell Gamma Knife calibration. *Med Phys*. 2010;37:5066–5071.
22. Kweon DC, Jae-Seung L, Eun-Hoe G, et al. An overall stem effect, including stem leakage and stem scatter, for a TM30013 farmer-type chamber. *J Korean Phys Soc*. 2011;58:1688.
23. Benmakhlouf H, Johansson J, Paddick I, Andreo P. Monte Carlo calculated and experimentally determined output correction factors for small field detectors in Leksell Gamma Knife Perfexion beams. *Phys Med Biol*. 2015;60:3959–3974.

24. Drzymala RE, Wood RC, Levy J. Calibration of the Gamma Knife using a new phantom following the AAPM TG51 and TG21 protocols. *Med Phys*. 2008;35:514–521.
25. Meltsner SG, DeWerd LA. Air kerma based dosimetry calibration for the Leksell Gamma Knife. *Med Phys*. 2009;36:339–350.
26. Chung JP, Seong YM, Kim TY, et al. Development of a PMMA phantom as a practical alternative for quality control of gamma knife® dosimetry. *Radiat Oncol Lond Engl*. 2018;13:176.